metals

MDPI

Article

Analysis of Shift in Nil-Ductility Transition Reference Temperature for RPV Steels Due to Irradiation Embrittlement Using Probability Distributions and Gamma Process

Kaikai Tang [1], Yan Li [1], Yuebing Li [1,2], Weiya Jin [1,2] and Jiameng Liu [1,2,*]

[1] College of Mechanical Engineering, Zhejiang University of Technology, Hangzhou 310032, China; tangkaikaitkktkk@126.com (K.T.); 2112102183@zjut.edu.cn (Y.L.); ybli@zjut.edu.cn (Y.L.); jinweiya@zjut.edu.cn (W.J.)

[2] Engineering Research Center of Process Equipment and Re-Manufacturing, Ministry of Education, Hangzhou 310032, China

* Correspondence: jiamengliu@zjut.edu.cn

Abstract: Reactor pressure vessel (RPV) steels are highly susceptible to irradiation embrittlement due to prolonged exposure to high temperature, high pressure, and intense neutron irradiation. This leads to the shift in nil-ductility transition reference temperature—ΔRT_{NDT}. The change in ΔRT_{NDT} follows a certain distribution pattern and is impacted by factors including chemical composition, neutron fluence, and irradiation temperature. Existing empirical procedures can estimate ΔRT_{NDT} based on fitting extensive irradiation embrittlement data, but their reliability has not been thoroughly investigated. Probability statistical distributions and the Gamma stochastic process were performed to model material property degradation in RPV steels from a pressurized water reactor due to irradiation embrittlement, with the probability models considered being normal, Weibull, and lognormal distributions. Comparisons with existing empirical procedures showed that the Weibull distribution model and the Gamma stochastic model demonstrate good reliability in predicting ΔRT_{NDT} for RPV steels. This provides a valuable reference for studying irradiation embrittlement in RPV materials.

Keywords: nil-ductility transition reference temperature; irradiation embrittlement; stepwise regression analysis; gamma process; probabilistic statistics

check for updates

Citation: Tang, K.; Li, Y.; Li, Y.; Jin, W.; Liu, J. Analysis of Shift in Nil-Ductility Transition Reference Temperature for RPV Steels Due to Irradiation Embrittlement Using Probability Distributions and Gamma Process. *Metals* **2024**, *14*, 580. https://doi.org/10.3390/met14050580

Academic Editor: Ferenc Gillemot

Received: 17 April 2024
Revised: 10 May 2024
Accepted: 12 May 2024
Published: 15 May 2024

Copyright: © 2024 by the authors. Licensee MDPI, Basel, Switzerland. This article is an open access article distributed under the terms and conditions of the Creative Commons Attribution (CC BY) license (https://creativecommons.org/licenses/by/4.0/).

1. Introduction

As irreplaceable core components of nuclear power plants, reactor pressure vessels (RPVs) endure prolonged neutron bombardment over their 60 to 80 years of service [1]. This continuous exposure leads to the gradual degradation of their material properties [2], manifesting as irradiation embrittlement. At the microscopic level, neutron irradiation causes the formation of defects such as vacancies, interstitial atom point defects, and clusters, which leads to the precipitation and segregation of solute atoms, notably with Cu-rich precipitates and P element segregation [3–5]. From a macroscopic perspective, RPV steels experience embrittlement, evidenced by an increase in nil-ductility transition reference temperature (RT_{NDT}) [5], a reduction in upper-shelf energy, and diminished fracture toughness.

Studies have revealed that the irradiation embrittlement of RPV steels is influenced by several factors, including irradiation temperature [6,7], neutron fluence [8–10], and chemical composition [11]. Edmondson et al. [12], Miller et al. [13], and Kuleshova et al. [14] explored the effects of low copper content (less than 0.1%) under high neutron fluence conditions on RPV steels. The shift in the nil-ductility transition reference temperature (ΔRT_{NDT}) serves as a critical indicator of irradiation embrittlement. Bing et al. [15] believed the irradiation embrittlement of RPV steels is primarily influenced by neutron fluence. He et al. [16] found, through fitting, that ΔRT_{NDT} increases rapidly with neutron fluence. Kryukov et al. [10]

investigated the effect of elements, finding that ΔRT_{NDT} gradually increases with neutron fluence and tends to stabilize.

To address the challenges related to the time and cost of irradiation experiments, empirical procedures based on the chemistry of steels (Cu and Ni contents) and the neutron fluence received have been developed for predicting ΔRT_{NDT}. Examples include RG1.99 (Rev.1), RG1.99 (Rev.2) [17], NUREG/CR [18,19], and ASME-E900 [20] from the United States; FIS [21] from France; and JEAC [22] from Japan. Given the diverse RPV materials used by different countries, the targeted elements for study vary accordingly. Specifically, France concentrates on Cu and P; the European Union and the United States prioritize Cu, P, and Ni [17]; and Japan focuses on Cu, P, Si, and Ni. At the same time, machine learning has been performed by numerous scholars to predict the performance of RPV steels [23–25]. This method, focusing on statistical theories rather than physical details, identifies optimal mathematical mappings between material properties and performance, showing significant strengths in addressing complex, coupled, and nonlinear issues. Castin et al. [26] used a three-layer artificial neural network to predict the radiation hardening of RPV steels. Following a similar approach, Mathew et al. [27] established a neural network-based model to forecast irradiation embrittlement of RPV steels. The trends predicted by both the machine learning-based model and the experience-based model are consistent, but they neglect the influence of alloy composition on the shift in RT_{NDT}. However, regardless of whether the approach is machine learning or a traditional empirical procedure, existing models are based on curves fitted from extensive experimental data, resulting in deterministic data that lack probabilistic reliability analysis. Given the requirements of probabilistic fracture mechanics for RPVs under various transients, such as pressurized thermal shock [28] and pressure–temperature limit curves [29], it is necessary to evaluate the uncertainty model of ΔRT_{NDT} due to irradiation.

Numerous methods for estimating reliability from degradation data have been proposed [30,31]. While degradation path modeling is commonly employed, it has limitations in handling time-varying systems and is effective only when randomness from environmental factors is negligible. Another approach involves stochastic process modeling, with the Wiener, Gamma, and Inverse Gaussian processes being the most commonly applied methodologies. The Gamma process model, as a degradation process, exhibits degradation monotonicity. It characterizes degradation increments by using the Gamma distribution and offers a reasonable physical interpretation for irreversible degradation phenomena. The Gamma process was first applied by Moran in a series of papers and a book published in the 1950s to simulate the process of water flowing into a dam [32]. In 1975, Abdel-Hameed [33] proposed using the Gamma process as a degradation model that occurs randomly over time. Over the past four decades, the Gamma process has consistently provided good fits to various types of data, including creep [34], fatigue crack growth [35], and corrosion thinning [36]. Lawless and Crowder [37] incorporated covariates and random effects into the degradation process model based on the Gamma process to characterize different degradation rates for different individuals and derived the distribution of failure time. In this paper, the Gamma process will be used to study the embrittlement behavior of RPV materials, and neutron fluence will be considered as a function of time to investigate ΔRT_{NDT}.

This paper aims to predict the shift in nil-ductility transition reference temperature (ΔRT_{NDT}) and explain the associated uncertainty based on probability distribution and the Gamma process. The distribution patterns of changed ΔRT_{NDT} under varied neutron fluences are analyzed from a probabilistic statistical perspective, and these changes are further derived from the perspective of stochastic degradation. The layout of this paper is as follows: The methodology for data processing and the theoretical framework of the prediction models are detailed in Section 2. The priority factors affecting ΔRT_{NDT} and the construction of prediction models are studied in Section 3. The comparative analysis of the prediction models, along with an evaluation against traditional empirical procedures, is discussed in Section 4. Key conclusions are presented in Section 5.

2. Methods

2.1. Data Collection and Processing

The research data were collected with two data sets. The first data set, containing 1707 data points, originated from the RPV irradiation embrittlement database POLTTER [38]. This data set was used to evaluate the impacts of various factors on irradiation embrittlement. The second data set, with 65 data points, was sourced from the database on the base materials of RPVs from pressurized water reactor nuclear power plants (900 Mwe) with neutron energy exceeding 1.0 MeV [39], which was provided by French company EDF. This data set was used to develop the prediction models with probability statistics and the Gamma process.

There are many factors that affect the irradiation embrittlement of RPV steel, such as the chemical element content [15] and irradiation conditions [40]. It is necessary to select important factors and eliminate unimportant factors. Therefore, stepwise regression analysis was used to assess the presence of any correlation between the eight predictors (the chemical composition of RPV steels: Ni, Mn, Si, P, Cu, and P; irradiation conditions: neutron fluence, neutron fluence rate, and irradiation temperature) and the shift in nil-ductility transition reference temperature (ΔRT_{NDT}; dependent variable) to identify the most influential factors on this parameter. Regression variables with different units were standardized firstly, and stepwise linear regression models were established as follows:

$$Y = \beta_0 + \beta_i X_i + \varepsilon \tag{1}$$

where Y is the dependent variable, X_i represents the independent variables ($1 \leq i \leq 8$), β_0 is the regression constant, β_i is the regression coefficient for each X_i, and ε is the error [41].

In regression analysis, variables are added or removed based on the significance level of the F-value (calculated by using Equation (2)), which was set at 0.05.

$$F = \frac{\sum_{i=1}^{n} (\hat{y}_i - \overline{y})^2 / m}{\sum_{i=1}^{n} (y_i - \hat{y}_i)^2 / n - m - 1} \tag{2}$$

where $\hat{y}_i$ is the regression value, y_i is the actual data value, $\overline{y}$ is the mean value of the actual data, m is the number of independent variables, n is the sample size, $\sum_{i=1}^{n} (\hat{y}_i - \overline{y})^2$ is the sum of squares of the regression, and $\sum_{i=1}^{n} (y_i - \hat{y}_i)^2$ is the sum of the squared error.

Then, to predict the irradiation embrittlement behavior of RPV steels, it is essential to initially analyze the variation in and distribution of the shift in nil-ductility transition reference temperature (ΔRT_{NDT}) within existing irradiated materials, as it serves as a crucial measure of irradiation embrittlement. The statistical analysis was conducted by using irradiation embrittlement sample data from RPV base materials at 288 °C irradiation temperature in pressurized water reactor nuclear power plants. The conventional calculation criteria for ΔRT_{NDT} also predominantly consider the dependence on three elements: Cu, Ni, and P. Combining with the above data, the range and average values of key elemental contents are listed in Table 1. Specifically, the Cu content ranges from 0.04 to 0.07 wt.%, the Ni content ranges from 0.66 to 0.75 wt.%, and the P content ranges from 0.005 to 0.009 wt.%. The mean values of 0.06 wt.%, 0.70 wt.%, and 0.007 wt.% for the elemental contents of Cu, Ni, and P, respectively, were used to estimate ΔRT_{NDT}, as reported in Section 4.

Considering the significant impact of neutron fluence on the shift in nil-ductility transition reference temperature (ΔRT_{NDT}), Figure 1 shows ΔRT_{NDT} for different neutron fluences, based on sample data. Overall, ΔRT_{NDT} tends to rise with the increase in neutron fluence. Moreover, at the same neutron fluence levels, there appears to be a certain distribution pattern observed for ΔRT_{NDT}.

Table 1. The ranges and average values of key elemental contents in RPV base materials.

Element	Minimum Value (wt.%)	Maximum Value (wt.%)	Mean Value (wt.%)
Cu	0.04	0.07	0.06
Ni	0.66	0.75	0.70
P	0.005	0.009	0.007

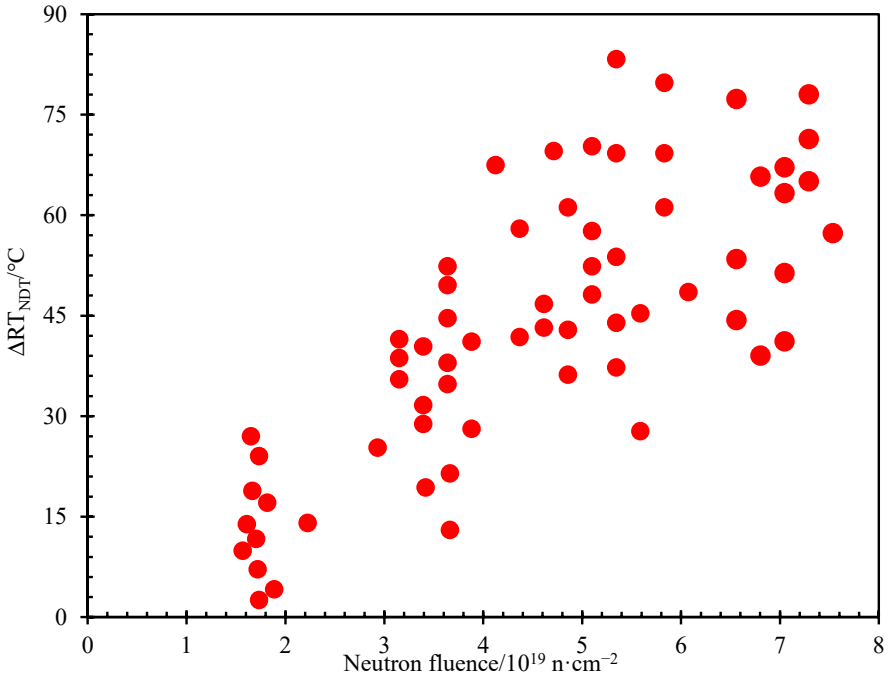

Figure 1. The shift in nil-ductility transition reference temperature (ΔRT_{NDT}) for different neutron fluences.

To deeply understand the distribution pattern of the shift in nil-ductility transition reference temperature (ΔRT_{NDT}) at the same neutron fluence levels, a crucial task is to ensure consistency across multiple data points of neutron fluence. Therefore, the K-means clustering algorithm was selected for data classification due to its ability to efficiently handle large-scale data sets [42]. The specific implementation steps are as follows:

Step 1: Divide n data points into k clusters, with each cluster selecting an initial cluster center.

Step 2: Apply the nearest-neighbor rule for clustering division [43], where each data point is assigned to the nearest cluster based on the minimum distance principle by using Equation (3) (also known as Euclidean distance).

$$d = \sqrt{(x - x_i)^2 + (y - y_i)^2} \tag{3}$$

where x_i and y_i are the coordinates of each cluster center.

Step 3: Update the cluster centers according to the sample mean of each cluster.

Step 4: Calculate the root mean square error between the new and old cluster centers for each cluster. If the error is less than the tolerance limit of 0.0001, then stop. Otherwise, return to step 2.

It is worth noting that when calculating the Euclidean distance by using Equation (3), only the distance between the horizontal coordinate points is calculated, while the vertical differences are ignored. This method is strategically chosen to foster a more vertically distributed configuration of the resulting clusters, aligning with the analytical objectives.

The data classification results under different cluster numbers are shown in Figure 2, where different colors represent distinct clusters. The green data are all identified as one

cluster due to their concentrated distribution along the vertical axis, while other data points, displaying greater dispersion along the horizontal axis, are challenging to classify. When the number of clusters, *K*, is small (Figure 2a), both the red and yellow clusters contain an excessive number of samples, resulting in reduced precision in the distribution fitting. As *K* increases, the degree of aggregation between data points within each cluster rapidly increases, leading to a noticeable improvement in clustering effectiveness (Figure 2b–d). However, when *K* is relatively large (Figure 2e,f), the categorization becomes overly granular, leading to an insufficient number of data points within each cluster. For example, the red and gray clusters contain only four data points each. This excessive subdivision increases the uncertainty in fitting the data rather than reducing it.

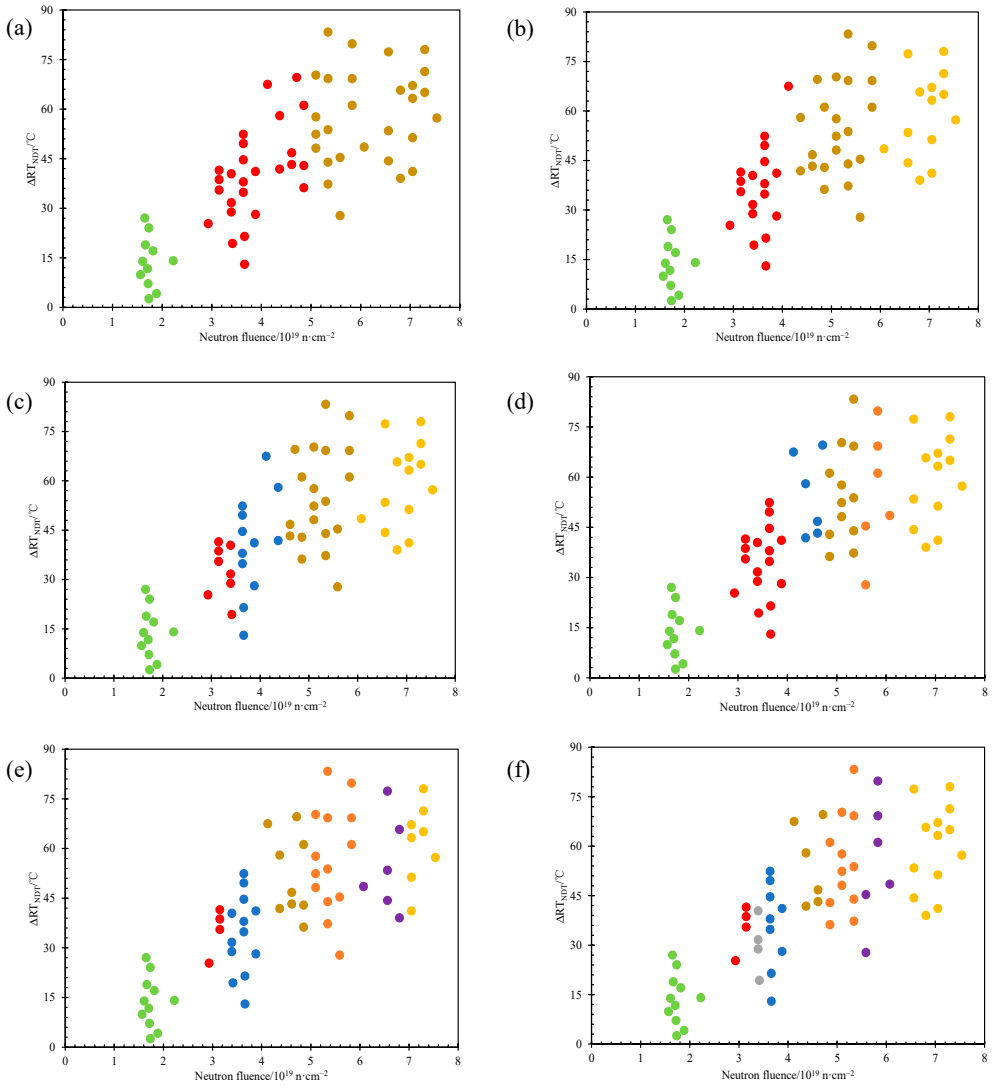

Figure 2. Cluster classification: (**a**) *K* = 3; (**b**) *K* = 4; (**c**) *K* = 5; (**d**) *K* = 6; (**e**) *K* = 7; (**f**) *K* = 8.

Within-Cluster Sum of Square (WCSS), which represents the sum of distances from each data point within a cluster to its corresponding cluster center, was calculated to select the most suitable value of *K*. The sum of squared errors (SSE) was calculated by Equation (4), and its relationship with the number of clusters is illustrated in Figure 3. Typically, the point of inflection where the decrease in the sum of squared errors is maximized and subsequently slows down is considered the optimal number of clusters. It can be observed that when the number of clusters increases from 3 to 4, there is a significant reduction in

intra-cluster distances. However, as K continues to increase, the change in SSE becomes less pronounced. Therefore, clusters with a K of 4 were chosen for subsequent analysis.

$$\mathrm{SSE} = \sum_{i=1}^{k} \sum_{p \in C_i} |p - m_i|^2 \tag{4}$$

where k is the number of cluster centers, C_i is the i-th cluster, p represents the neutron fluence of data points in the i-th cluster, and m is the neutron fluence of the cluster center point (vertical distance is ignored).

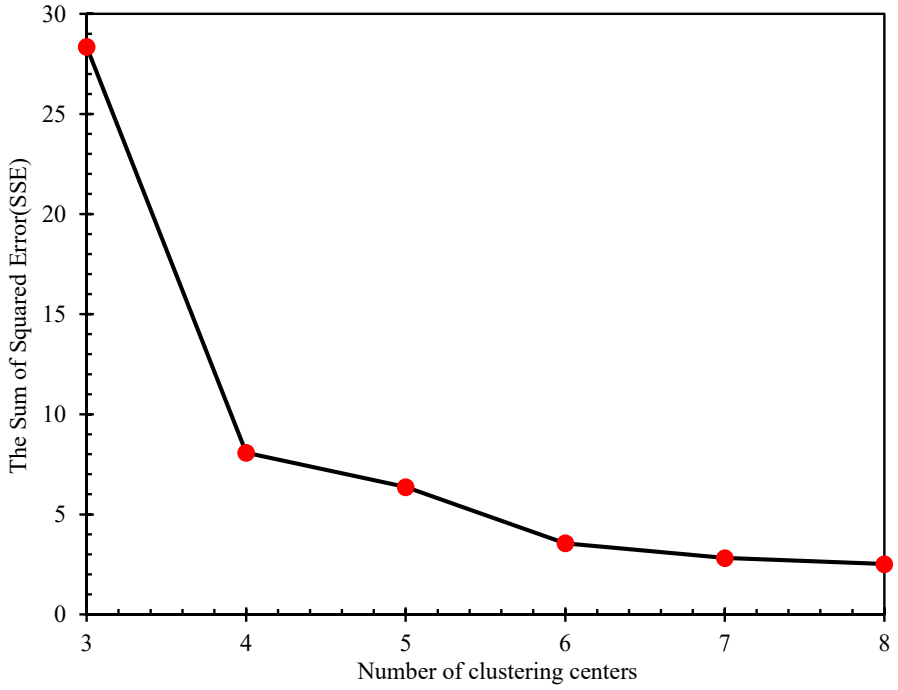

Figure 3. Relation between the number of clusters and the sum of squared errors.

2.2. Prediction by Probability Statistical Models

After analyzing and processing the data from the second data set, each group of data was subjected to statistical distribution fitting, and the common distributions lognormal, normal, and Weibull were applied to fit the left-skewed sample data. Then, the distribution parameters of the probabilistic statistical models were analyzed for the shift in nil-ductility transition reference temperature (ΔRT_{NDT}) at 4 neutron fluence levels. The cumulative probability functions ($F(t)$) for the 3 distributions are provided by Equations (5)–(7), where t refers to ΔRT_{NDT}. Specifically, to determine the distribution parameters for the prediction models, the y-axis values (ΔRT_{NDT}) of the clustered data were systematically sorted from the lowest to the highest, and the Hensen formula was used to establish the relationship between the values of ΔRT_{NDT} and the cumulative probability functions of each data point, as shown in Equation (8).

$$\text{lognormal distribution } F(t) = \int_0^t \frac{1}{\sqrt{2\pi}\sigma x} e^{-\frac{1}{2}\left(\frac{\ln x - \mu}{\sigma}\right)^2} \tag{5}$$

$$\text{normal distribution } F(t) = \int_0^t \frac{1}{\sqrt{2\pi}\sigma} e^{-\frac{1}{2}\left(\frac{x-\mu}{\sigma}\right)^2} dx \tag{6}$$

$$\text{Weibull distribution } F(t) = 1 - e^{-\left(\frac{t}{\eta}\right)^m} \tag{7}$$

$$\text{Hansen formula } F_n(t_i) = (i - 0.5)/n \tag{8}$$

where μ is the mean value, σ is the standard deviation, m is the shape parameter, η represents the characteristic lifetime or true scale parameter, i is the rank, and n is the sample size.

The root mean square error (RMSE) was introduced to evaluate the fitting effectiveness and determine the optimal probability distribution of the 3 distribution models with Equation (9). A larger RMSE value indicates poorer fitting performance.

$$\mathrm{RMSE} = \sqrt{\frac{1}{\mathrm{n}}\sum_{\mathrm{i}=1}^{n}\left(Y_{test_i} - Y_{predict_i}\right)^2} \tag{9}$$

where Y_{test_i} is the test data value of the i-th $\Delta\mathrm{RT_{NDT}}$ corresponding to a neutron fluence from the database and $Y_{predict_i}$ is the predicted value of the i-th $\Delta\mathrm{RT_{NDT}}$ obtained from the prediction models.

2.3. Prediction by Gamma Stochastic Process Model

On the other hand, the impact of time on the degradation of the mechanical properties of RPV steels was considered. After neutron irradiation, the shift in the nil-ductility transition reference temperature ($\Delta\mathrm{RT_{NDT}}$) of RPV steels exhibits a gradual upward trend with the increase in neutron fluence, characterized by both randomness and irreversibility. The process of $\Delta\mathrm{RT_{NDT}}$ variation is well suited for analysis using the Gamma process, which features independent and non-negative increments [30]. This allows for the quantification of the degradation process of RPV steels after neutron irradiation. Given the influence of chemical elements on the shift in nil-ductility transition reference temperature ($\Delta\mathrm{RT_{NDT}}$), this effect was here transformed into a stochastic impact of neutron fluence on $\Delta\mathrm{RT_{NDT}}$.

If the shift in nil-ductility transition reference temperature $x(t)$ of RPV steels follows a Gamma process [31], that is, $x(t) \sim Ga(t; v, u)$, where $x(0) = 0$, t represents neutron fluence rather than time, v is the deterministic shape parameter, and u is the random scale parameter, the cumulative probability function of the shift in the nil-ductility transition reference temperature ($\Delta\mathrm{RT_{NDT}}$) of RPV steels caused by neutron irradiation is given by Equation (10).

$$\mathrm{Ga}(x|v,u) = \frac{u^v x^{v-1}\exp(-ux)}{\Gamma(v)} I_{0,\infty}(x) \tag{10}$$

where $\Gamma(v)$ is the gamma function, $\Gamma(v) = \int_0^\infty t^{v-1}e^{-t}dt$, and $I_{0,\infty}(x) = \begin{cases} 1 & x \in (0,\infty) \\ 0 & x \notin (0,\infty) \end{cases}$.

In any neutron fluence interval (f_i, f_j), the change in $\Delta\mathrm{RT_{NDT}}$ follows a distribution denoted by $\Delta R_{ij} \sim Ga\left[v(f_i) - v(f_j), u\right]$. Based on the properties of the Gamma process, the expected value (mean value) ($E(x(t))$) and variance ($Var[x(t)]$) of $\Delta\mathrm{RT_{NDT}}$ are calculated by using Equations (11) and (12), respectively, and the relationship between the expected value and variance with scale parameter u is given by Equation (13). It is important to highlight that when fitting the cluster centers obtained from the K-means clustering algorithm (as described in Section 2.1), $\Delta\mathrm{RT_{NDT}}$ increases with the neutron fluence, as shown in Figure 4. Therefore, shape parameter v is regarded as a linear function of the neutron fluence, that is, $v = at$, where the expression for a is provided by Equation (14).

$$E\left(\Delta R_{ij}\right) = \frac{a\left(f_i - f_j\right)}{u} \tag{11}$$

$$Var\left(\Delta R_{ij}\right) = \frac{a\left(f_i - f_j\right)}{u^2} \tag{12}$$

$$u = \frac{E\left(\Delta R_{ij}\right)}{Var\left(\Delta R_{ij}\right)} \tag{13}$$

$$a = \frac{u^2\left[E\left(\Delta R_{ij}\right) + Var\left(\Delta R_{ij}\right)\right]}{(f_i - f_i)(u+1)} \tag{14}$$

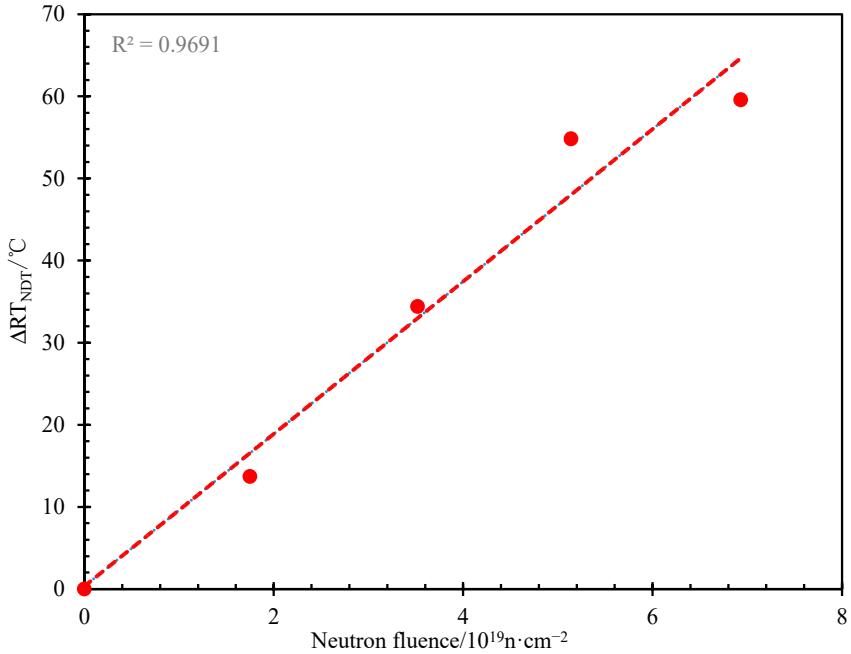

Figure 4. The fitting curve between the shift in nil-ductility transition reference temperature (ΔRT_{NDT}) and neutron fluence.

Before parameter estimation, it is necessary to obtain sufficient data samples regarding the change in the shift in nil-ductility transition reference temperature (ΔRT_{NDT}). Based on the fitted curve, neutron fluence was divided into 14 intervals in the range [0.5, 1], [1, 1.5], . . ., [6.5, 7]. The linear interpolation method was applied to obtain the value of ΔRT_{NDT} at each interval point, thereby calculating the change in ΔRT_{NDT} within these ranges. Since the maximum neutron fluence in the original samples is only 7.3×10^{19} n·cm^{-2}, the maximum value of the intervals was controlled at 7×10^{19} n·cm^{-2} to ensure the reliability of the data.

3. Results

3.1. Impact Factor Analysis

The regression model coefficients and test results are listed in Table 2. The neutron fluence rate was excluded from the model due to its lack of significance. Typically, when the *p*-value is less than 0.05, the independent variable is considered significant for the model [44]. It can be observed that the chemical composition, neutron fluence, and irradiation temperature all have an impact on the shift in nil-ductility transition reference temperature (ΔRT_{NDT}). Higher coefficient values (β) suggest a stronger influence on this increment, regardless of their positive or negative signs. For a variable with a negative standardized coefficient, such as irradiation temperature, its effect on ΔRT_{NDT} is negative. The absolute values of the standardized coefficients for each variable are shown in Figure 5. The collinearity diagnostic results indicate that the Variance Inflation Factor (VIF) is below 1, significantly lower than the threshold value of 10. Moreover, the tolerance values approach 1, suggesting minimal multicollinearity issues among the independent variables in this model. Furthermore, the reliability of the regression model was evaluated by using the F-test, the coefficient of determination (R^2), and the Durbin–Watson (D-W) test. The results indicate that the model fits well ($R^2 = 0.676$) and has statistical significance ($F = 505.777$, $p < 0.001$). The D-W value closer to 2 indicates a greater assurance of no autocorrelation in the regression residuals. The results demonstrate that the error terms of the model are independent, and the regression model is reliable (D-W = 1.077).

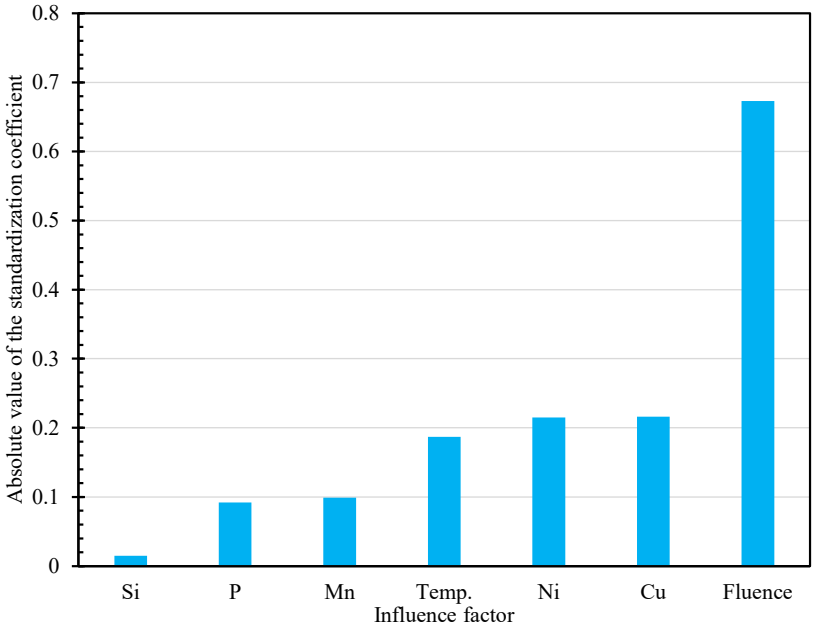

Figure 5. Priority of impact factors.

Table 2. The coefficients and test results of the stepwise regression analysis (n = 1707).

	Unstandardized Coefficients		Standardized Coefficients	*t*	*p*	Collinearity Diagnostics	
	B	Standard Error	*β*			VIF	Tolerance
Constant	144.975	13.640	-	10.628	0.000	-	-
Ni (w%)	20.083	1.358	0.215	14.784	0.000	1.104	0.906
Mn (w%)	9.769	1.424	0.099	6.862	0.000	1.087	0.920
Si (w%)	5.061	4.937	0.015	1.025	0.305	1.051	0.951
P(w%)	294.988	45.152	0.092	6.533	0.000	1.044	0.958
Cu (w%)	215.541	14.233	0.216	15.144	0.000	1.071	0.934
Fluence [n/cm^2]	0.000	0.000	0.673	46.739	0.000	1.086	0.920
Temperature [°C]	−0.611	0.046	−0.187	−13.271	0.000	1.039	0.962
R				0.676			
F				F(7,1699) = 505.777, p = 0.000			
D-W				1.077			

As seen in Figure 5, neutron fluence has the most significant positive impact on ΔRT_{NDT}, thereby greatly influencing the irradiation embrittlement of RPV steels. Additionally, the chemical composition affects irradiation embrittlement, with Cu, Ni, Mn, P, and Si showing decreasing levels of impact in sequence, and Si content shows minimal to negligible effects on irradiation embrittlement. Considering the significant influence of neutron fluence, the probability distribution of the shift in nil-ductility transition reference temperature at different neutron fluence levels was analyzed and predicted, as shown in Section 3.2. The irradiation embrittlement model incorporating the stochastic effect of neutron fluence was established and is discussed in Section 3.3.

3.2. Probability Statistical Model

For reliability values of 5%, 50%, and 95%, the fitting results for normal, Weibull, and lognormal distributions are shown in Figure 6. The detailed data can be found in Table 3. The results indicate that the fitting performance of the lognormal distribution is significantly inferior to that of the Weibull distribution and normal distribution. However, the difference between the Weibull distribution and the normal distribution is not significant, and further analysis is needed.

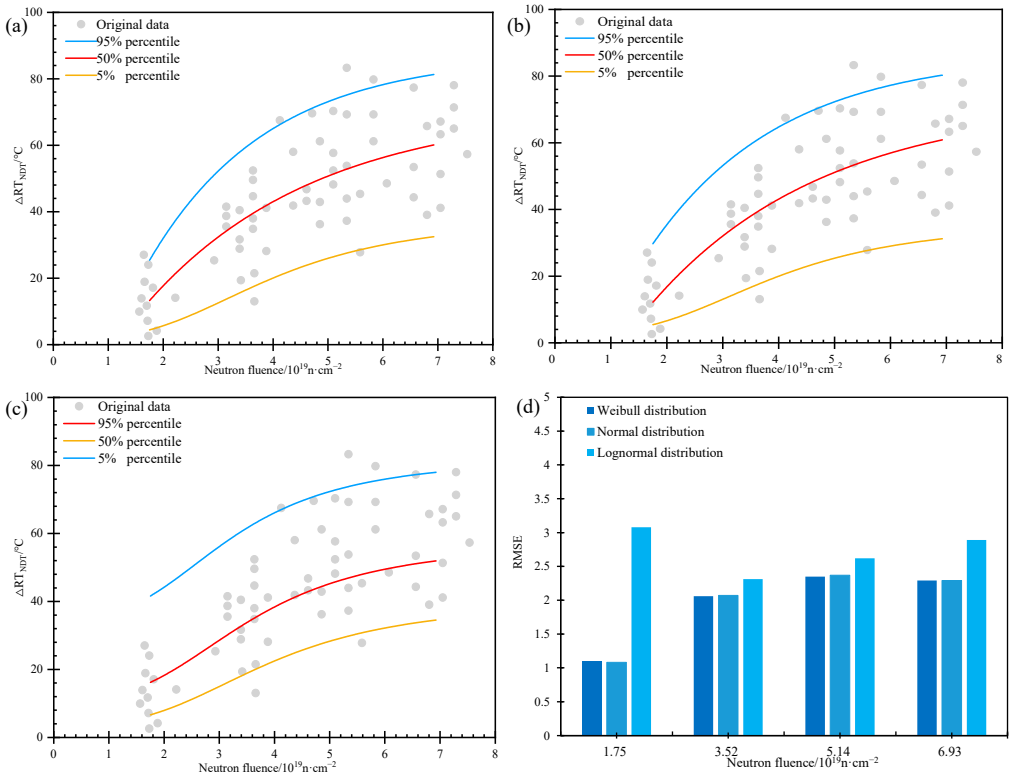

Figure 6. The fitting curves and root mean square error (RMSE) diagrams for the three distributions: (**a**) normal distribution; (**b**) Weibull distribution; (**c**) lognormal distribution; (**d**) RMSE comparison diagrams.

Table 3. Data in different distributions and reliability values.

Neutron Fluence/10^{19}·n cm^{-2}		**1.75**	**3.52**	**5.14**	**6.93**
Normal distribution	5%	1.58	15.48	30.86	38.41
	50%	13.71	36.24	54.52	58.80
	95%	25.85	57.01	78.19	79.19
Lognormal distribution	5%	3.63	18.13	33.59	40.08
	50%	11.28	33.91	52.59	57.45
	95%	35.09	63.41	82.33	82.33
Weibull distribution	5%	2.67	15.78	30.38	36.44
	50%	12.61	36.07	55.02	59.55
	95%	30.16	57.41	76.82	78.49

To predict the variation in ΔRT_{NDT} at other neutron fluence levels, the relationship between the parameters of the Weibull distribution and normal distribution (denoted by y) and the neutron fluence (denoted by x) was studied. Due to the inconvenience of calculating coefficients with neutron fluence values of 10^{19}, the existing four neutron fluence cluster values were normalized by using Equation (15) to fall within the range [0, 1], with x_{max} of 7.5×10^{19} n·cm^{-2}.

$$x = \frac{x}{x_{max}} \tag{15}$$

Figure 7 shows the fitted curves of Weibull distribution parameters and normal distribution parameters with different neutron fluences. The four points on the plot represent the actual values of distribution parameters at known neutron fluences, and the dashed lines represent the fitting curves. The coefficient of determination (R^2) reflects the goodness-of-fit of these curves. The R^2 for the curves of the four distribution parameters are 0.983 (μ), 0.9903 (σ^2), 0.988 (m), and 0.9814 (η), all approaching 1.0. This indicates strong interpretabil-

ity of the curves and excellent fitting performance. The expressions of the distribution parameters are detailed in Table 4.

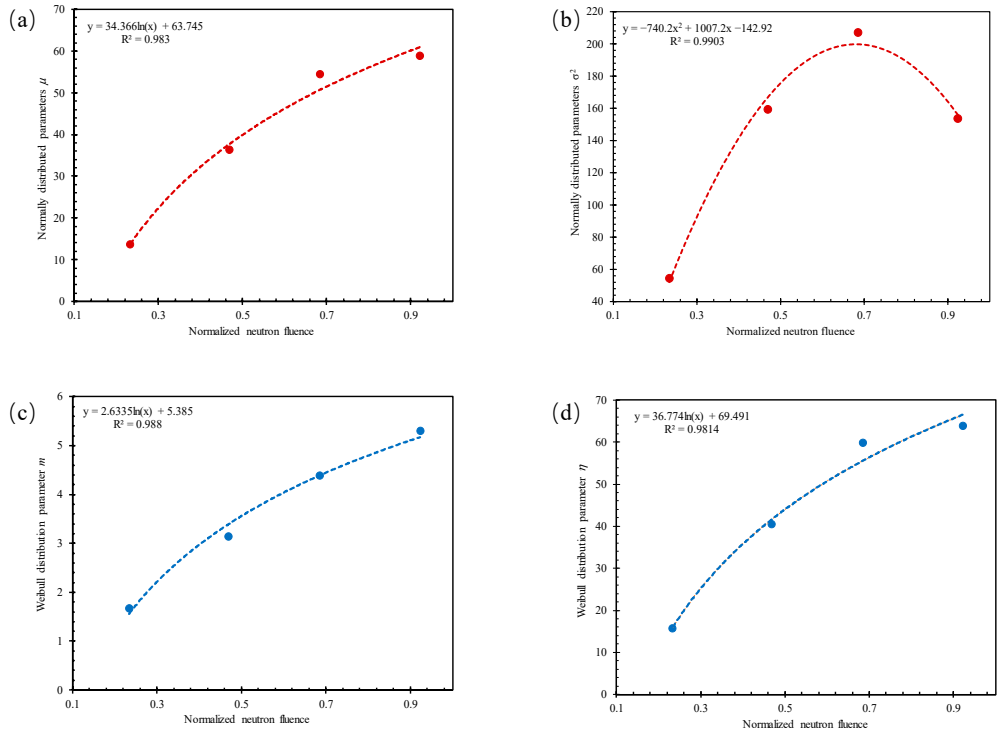

Figure 7. The fitting curves of Weibull distribution parameters and normal distribution parameters with neutron fluence: (**a**) normal distribution parameter μ; (**b**) normal distribution parameter σ^2; (**c**) Weibull distribution shape parameter m; (**d**) Weibull scale parameter η.

Table 4. The expressions of the four distribution parameters.

Type	Parameter	Parameter Equation
Normal distribution	μ	$\mu = 34.366\ln(x) + 63.745$
	σ^2	$\sigma^2 = -740.2x^2 + 1007.2x - 142.92$
Weibull distribution	m	$m = 2.6335\ln(x) + 5.385$
	η	$\eta = 36.774\ln(x) + 69.491$

The neutron fluence data from the POLTTER database in Section 2.1 were selected to validate the accuracy of both the Weibull distribution model and the normal distribution model. The cumulative probability function curves for neutron fluences of 2.46×10^{19} n·cm^{-2} and 4.75×10^{19} n·cm^{-2} are shown in Figure 8. The y-axis represents the probability of material failure, where ΔRT_{NDT} is less than or equal to a specific value. From Figure 8, it can be seen that at a neutron fluence of 2.46×10^{19} n·cm^{-2}, when ΔRT_{NDT} is approximately below 30 °C (Figure 8a), the cumulative probability function ($F(t)$) of the predicted values exceeds that of the test data values. Similarly, at a neutron fluence of 4.75×10^{19} n·cm^{-2}, when ΔRT_{NDT} is below 40 °C (Figure 8b), the same trend is observed. Thus, in both scenarios, the predicted values obtained from the prediction models exhibit a higher failure probability compared with the test data values, indicating a more conservative estimation at the same ΔRT_{NDT} values. Furthermore, in high-probability situations ($F(t) > 0.8$), the predicted values of ΔRT_{NDT} are higher than the test data values. This implies a larger increment in the nil-ductility transition reference temperature, bringing RT_{NDT} closer to the safety threshold assumed for RPV failure. Consequently, the service life of the material is shortened, resulting in a more conservative estimation.

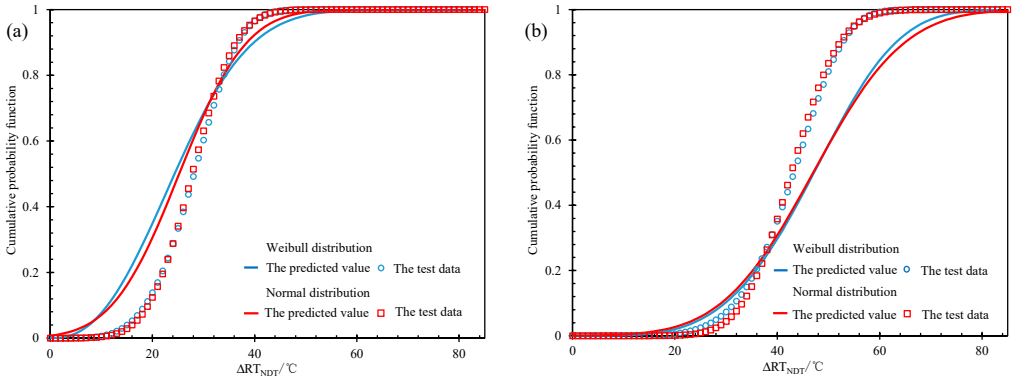

Figure 8. The curves of the cumulative probability function ($F(t)$) for two neutron fluences: (**a**) 2.46 × 10^{19} n·cm^{-2}; (**b**) 4.75 × 10^{19} n·cm^{-2}.

The cross-entropy between predicted and test data values under different probability distribution functions was calculated by using Equation (16). The results indicate that at a neutron fluence of 2.46 × 10^{19} n·cm^{-2}, the cross-entropy values for the Weibull and normal distributions are 3.598 and 3.926, respectively. Similarly, at a neutron fluence of 4.75 × 10^{19} n·cm^{-2}, the values are 3.750 and 4.377, respectively. A smaller cross-entropy value indicates a higher degree of conformity between the two distributions, suggesting that the Weibull distribution provides a better fit for the prediction model.

$$H(p,q) = -\sum_{x} p(x) \log q(x) \tag{16}$$

where $p(x)$is the probability distribution of the test data values, $q(x)$is the probability distribution of the predicted values, and x represents the specific value of ΔRT_{NDT}.

The RMSEs between the predicted values from the two distribution models and the test data values were calculated, as shown in Figure 9. The Weibull distribution has a smaller RMSE compared with the normal distribution. Furthermore, the trend of the Weibull distribution parameters is more uniquely determined, indicating higher reliability of the estimation method, which is more suitable for engineering applications. Therefore, it is recommended to use the Weibull distribution for predicting the shift in nil-ductility transition reference temperature that changes with neutron irradiation.

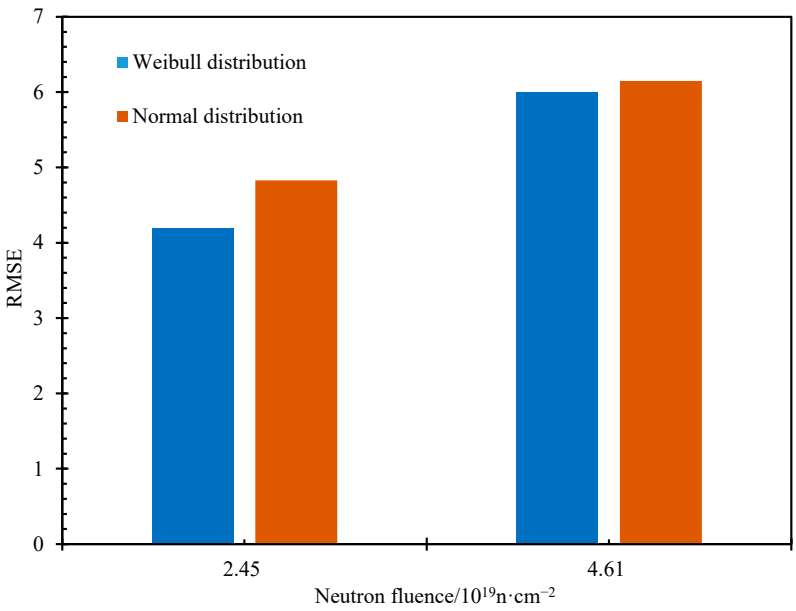

Figure 9. RMSE results of the two distribution models after prediction.

3.3. Gamma Stochastic Model

According to the parameter estimation method for the Gamma process, the data results are listed in Table 5.

Table 5. The results of linear interpolation for the change in ΔRT_{NDT}.

Neutron Fluence 10^{19} n/cm^2	ΔRT_{NDT} /°C	Change in ΔRT_{NDT} /°C
0.5	3.910	3.910
1	7.820	3.910
1.5	11.730	3.910
2	16.661	4.931
2.5	22.641	5.980
3	28.621	5.980
3.5	34.601	5.980
4	40.796	6.196
4.5	46.985	6.189
5	53.173	6.189
5.5	55.759	2.586
6	57.043	1.284
6.5	58.327	1.284
7	59.611	1.284

The data obtained from Table 5 were substituted into Equations (10)–(13); combined with the parameter estimation method for the Gamma process, the mean value (E) and variance (Var) were calculated to be 4.256 and 3.865, respectively. Gamma distribution parameters u and v were then obtained as per Equation (17).

$$\begin{cases} u = 1.102 \\ v = 9.381t \end{cases} \tag{17}$$

The predicted values obtained from the Gamma stochastic process were compared with the test data values, and the cumulative probability functions under different neutron fluences are shown in Figure 10. The cumulative probability function of the test data values was calculated by using the Weibull distribution parameters from Section 3.2. Specifically, six neutron fluences were considered, including the four neutron fluences obtained after clustering and other neutron fluences selected from the POLTTER database (as mentioned in Section 2). When the cumulative probability exceeds 0.3 (i.e., the 30% percentile), the errors between the predicted values and the test data values for different neutron fluences are below 20%, except for the neutron fluence of 6.93×10^{19} n·cm^{-2}, reflecting the reliability of the stochastic model at high and medium quantile points. Enhancing the model's reliability at low quantile points will be a focus of future research. Specifically, at the neutron fluence of 6.93×10^{19} n·cm^{-2} (Figure 10f), the predictive performance of the model based on the Gamma stochastic process is poor, possibly due to the neutron fluence approaching the maximum value at the edge.

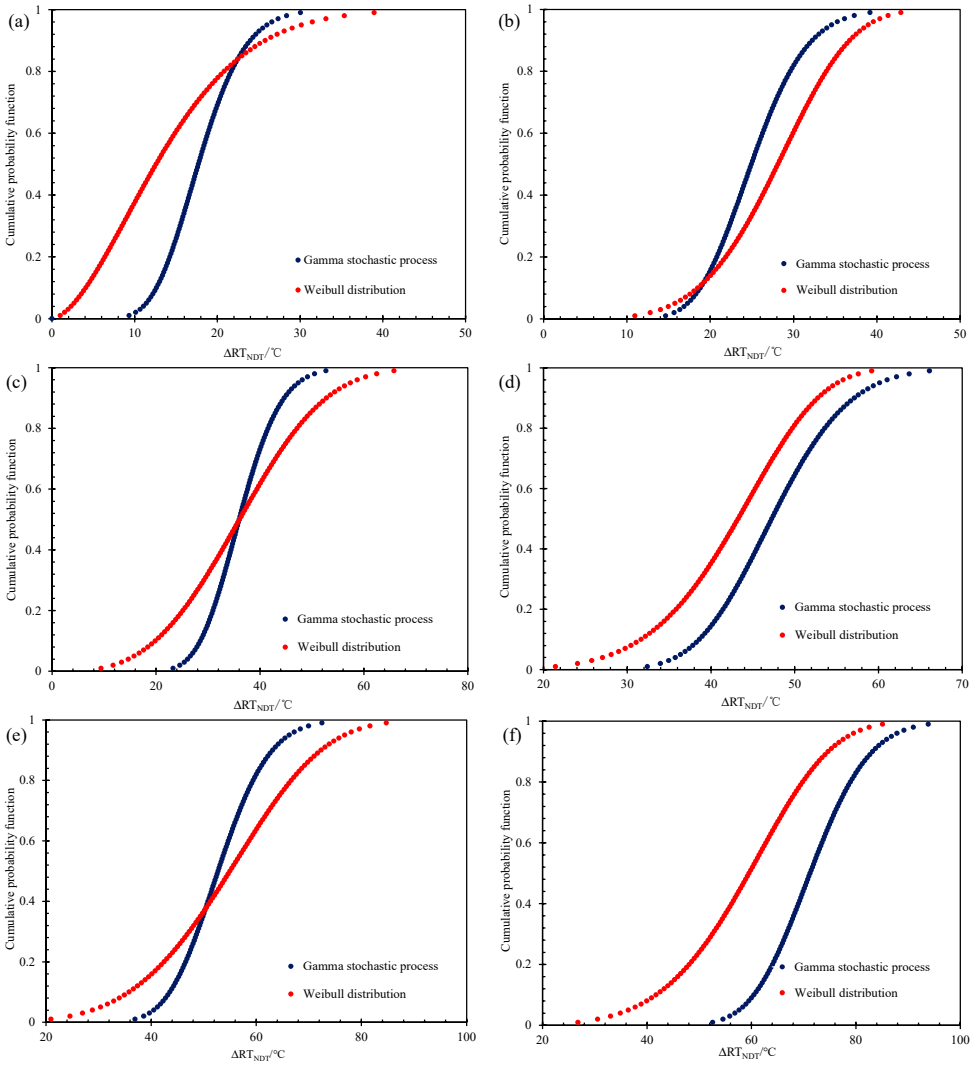

Figure 10. Cumulative probability function ($F(t)$) for different neutron fluences: (**a**) 1.75×10^{19} n·cm^{-2}; (**b**) 2.45×10^{19} n·cm^{-2}; (**c**) 3.52×10^{19} n·cm^{-2}; (**d**) 4.61×10^{19} n·cm^{-2}; (**e**) 5.14×10^{19} n·cm^{-2}; (**f**) 6.93×10^{19} n·cm^{-2}.

4. Discussion

4.1. Comparison with Probability Statistical Model and Stochastic Process

Considering the 5%, 50%, and 95% percentiles, the relationship between ΔRT_{NDT} and neutron fluence was explored by using both the Gamma stochastic process and the Weibull distribution prediction models, as shown in Figure 11. When the reliability reaches the 50% percentile and above, the predicted values of the two models are close. However, at lower percentiles (Figure 11a), the Gamma process predicts higher values than the Weibull distribution, suggesting a more conservative estimation.

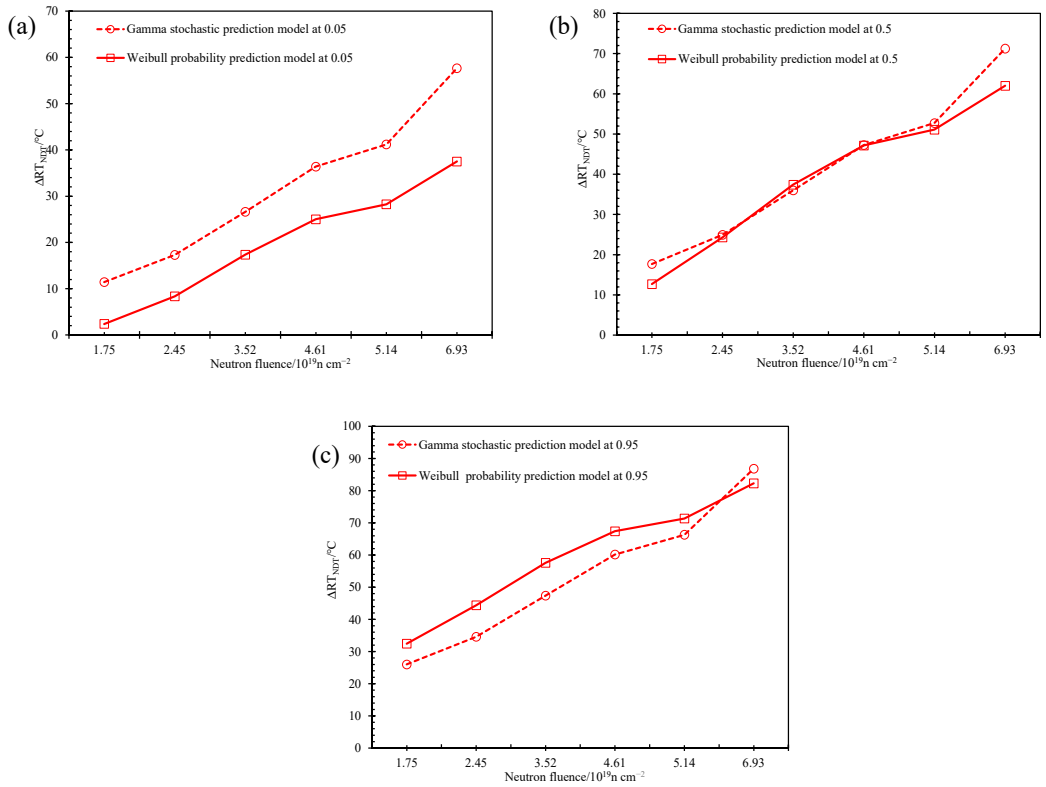

Figure 11. Comparison between the Gamma process and the Weibull distribution models' predictions: (**a**) 5%; (**b**) 50%; (**c**) 95%.

4.2. Comparison with Empirical Prediction Models

The shift in nil-ductility transition reference temperature (ΔRT_{NDT}) can be obtained by the Charpy pendulum impact test. Various countries have developed empirical procedures to predict ΔRT_{NDT} based on test results. Notable examples include French FIS [21], Japanese JEAC-4201 [22], American RG1.99-Rev2 [18], and the American ASTM model. These models provide expressions for calculating ΔRT_{NDT}, as presented in Equations (18)–(21).

French FIS:

$$\Delta RT_{NDT} = 8 + \left[\begin{array}{l} 24 + 238(Cu - 0.008) + \\ 1537(P - 0.008) + 19Ni^2 \times Cu \end{array} \right] \left[\frac{f}{10^{19}} \right]^{0.35} \quad (18)$$

Japanese JEAC-4201:

$$\begin{array}{rl} \Delta RT_{NDT} & = \left[-16 + 1210P + 215Cu + 77\sqrt{Cu \times Ni} \right] \\ & \times f^{0.29 - 0.04 \log f} (^{\circ}C) \end{array} \quad (19)$$

American RG1.99-Rev2:

$$\Delta RT_{NDT} = (CF) f^{(0.28 - 0.10 \log f)} \quad (20)$$

American ATSM-E900:

$$\left\{ \begin{array}{l} TTS = TTS_1 + TTS_2 \\ TTS_1 = A \times \frac{5}{9} \times 1.8943 \times 10^{-12} \cdot \Phi^{0.5695} \left(\frac{1.8T + 32}{550} \right)^{-5.47} \\ \quad \left(0.09 + \frac{P}{0.012} \right)^{0.216} \left(1.66 + \frac{N_i^{8.54}}{0.63} \right)^{0.39} \left(\frac{Mn}{1.36} \right)^{0.3} \\ TTS_2 = \frac{5}{9} \times \max[\min(Cu, 0.28) - 0.053, 0] \times M \\ M = B \times \max\{\min[113.87(\ln(\Phi) - \ln(4.5 \times 10^{20})), 612.6], 0\} \cdot \\ \quad \left(\frac{1.8T + 32}{550} \right)^{-5.45} \left(0.1 + \frac{P}{0.012} \right)^{-0.098} \left(0.168 + \frac{N_i^{0.58}}{0.63} \right)^{0.73} \end{array} \right. \quad (21)$$

where f and Φ represent neutron fluence in n/cm^2 and n/m^2 (E > 1 MeV), T is the irradiation temperature in °C, $A = \begin{pmatrix} 1.011 & \text{for forgings} \\ 1.080 & \text{for plates and SRM plates} \\ 0.919 & \text{for welds} \end{pmatrix}$, and $B = \begin{pmatrix} 0.738 & \text{for forgings} \\ 0.819 & \text{for plates and SRM plates} \\ 0.968 & \text{for welds} \end{pmatrix}$.

In the empirical procedures, the irradiation temperature was set to 288 °C, and the contents of Cu, P, and Ni were taken as 0.06 wt.%, 0.70 wt.%, and 0.007 wt.%, respectively (as described in Section 2). *CF* was determined to be 37 according to the standard.

Since test results have often been converted into mean values to determine the formulas, data in the 50% percentile were selected for both the Weibull distribution and Gamma stochastic process prediction models. The predicted values from these two models were compared with the predictions obtained from existing empirical procedures, and the results are shown in Figure 12. The ΔRT_{NDT} predicted by both models accelerates rapidly with the increase in neutron fluence, while the curve obtained from the empirical procedures is more gradual. The difference can be attributed to the traditional empirical procedures giving more weight to chemical element and placing less emphasis on the neutron fluence factor during data fitting. According to the priority analysis of factors influencing ΔRT_{NDT} (Figure 5), the importance of neutron fluence should far exceed that of elemental composition.

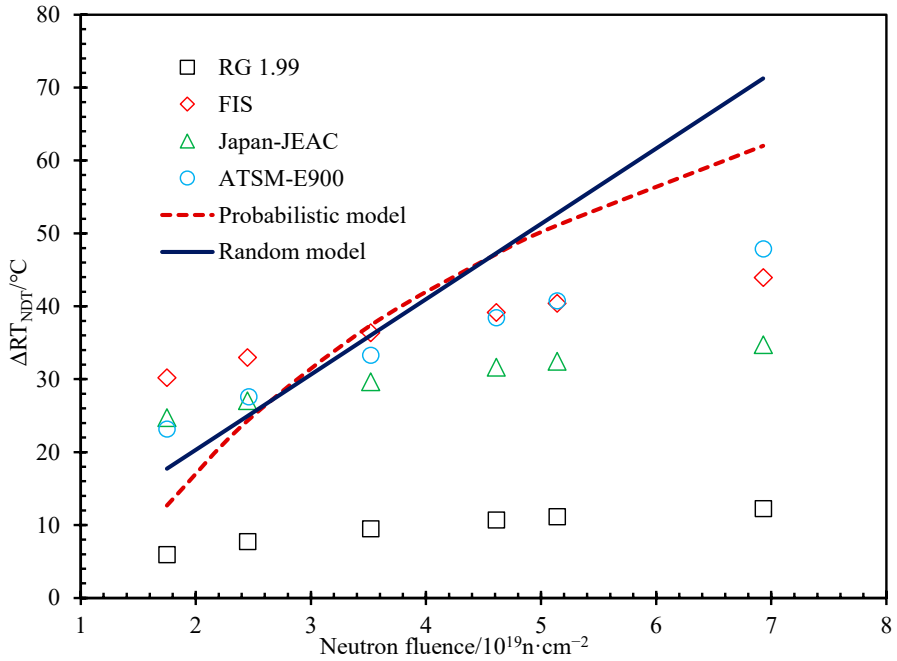

Figure 12. Comparison of values of ΔRT_{NDT} predicted by the Weibull distribution model, Gamma process model, and empirical procedures.

Though the predicted values of ΔRT_{NDT} from our model exceed those derived from empirical procedures under high-neutron-fluence conditions, this discrepancy is consistent with documented behaviors of steel under specific irradiation conditions, rather than being an anomaly. To support our results, we refer to several key studies that align with our observations and further validate the accuracy and applicability of our model. Kuleshova et al. has shown that for 15Kh2NMFAA steel, when subjected to an irradiation temperature of 300 °C and a neutron fluence of 4.5 × 10^{19} n·cm^{-2}, the ΔRT_{NDT} value reaches 46 °C [6]. This figure notably surpasses the fitting values yielded by conventional empirical procedures, which stay below 40 °C. Similarly, Wan et al. have found that for the base material at a high neutron fluence of 5.24 × 10^{19} n·cm^{-2}, the maximum ΔRT_{NDT}

value observed is 83 °C. For weldments, with a neutron fluence of 7.26×10^{19} n·cm^{-2}, the highest ΔRT_{NDT} value recorded is 89 °C [39], significantly exceeding the predictions of empirical procedures. These findings indicate that under certain conditions, the ΔRT_{NDT} value can indeed be higher than those traditionally predicted. Furthermore, Kryukov's work on WWER-440 steel supports our model's findings. For high neutron fluences, the rate of increase in ΔRT_{NDT} with neutron fluence rises sharply [10], aligning with the trend observed in our model. This alignment further strengthens the credibility of our model. Therefore, we believe that the two prediction models still maintain high reliability.

5. Conclusions

In this paper, a stepwise analysis method was used to prioritize factors influencing the shift in nil-ductility transition reference temperature (ΔRT_{NDT}). Subsequently, the relationship between neutron fluence and ΔRT_{NDT} was studied. By using the K-means algorithm, ΔRT_{NDT} values for different neutron fluence levels were clustered to form cluster centers. Three probability distribution models, including normal, Weibull, and lognormal distributions, were then fitted to determine the distribution parameters and predict ΔRT_{NDT} at a given neutron fluence. Considering the random effects of chemical elements, the Gamma stochastic process was applied to predict ΔRT_{NDT}, and the parameters of the Gamma distribution were fitted accordingly. The results of ΔRT_{NDT} predicted by the models were compared with those obtained by existing empirical procedures. This study provides a certain reference for predicting ΔRT_{NDT} based on neutron fluence. Key conclusions are as follows.

(1) Neutron fluence, chemical elements, and irradiation temperature all influence the ΔRT_{NDT}. Neutron fluence has a significant impact on ΔRT_{NDT} compared with chemical elements, while irradiation temperature negatively affects it.

(2) The lognormal distribution was excluded due to its large root mean square error in fitting. Comparison with test data revealed that the Weibull distribution model is more suitable for engineering applications compared with the normal distribution model.

(3) The prediction models based on the Weibull distribution and the Gamma process both exhibit a degree of reliability. The predicted values of ΔRT_{NDT} obtained by the prediction models are larger than the results of the empirical procedure under the high-neutron-fluence conditions, indicating an increased level of conservatism. This conservative bias underscores the superiority of prediction models in enhancing the rigor of security assessments. For practical engineering purposes, it is advisable to adopt the conservative estimates provided by both models as reference values.

Author Contributions: Conceptualization, Y.L. (Yuebing Li) and J.L.; Data curation, K.T.; Funding acquisition, Y.L. (Yuebing Li); Methodology, K.T. and J.L.; Project administration, W.J.; Software, K.T.; Supervision, J.L.; Validation, W.J.; Writing—original draft, K.T. and Y.L. (Yan Li); Writing—review and editing, Y.L. (Yan Li) and Y.L. (Yuebing Li). All authors have read and agreed to the published version of the manuscript.

Funding: This project was supported by the National Natural Science Foundation of China (52375161).

Data Availability Statement: The raw data supporting the conclusions of this article will be made available by the authors on request.

Conflicts of Interest: The authors declare no conflicts of interest.

References

1. Yuya, H.; Yabuuchi, K.; Kimura, A. Radiation embrittlement of clad-HAZ of RPV of a decommissioned BWR plant. *J. Nucl. Mater.* **2021**, *557*, 153300. [CrossRef]
2. Odette, G.R.; Lucas, G.E. Embrittlement of Nuclear Reactor Pressure Vessels. *JOM* **2001**, *53*, 18–22. [CrossRef]
3. Fedotova, S.; Kuleshova, E. The Effect of Operational Factors on Phase Formation Patterns in the Light-Water Reactor Pressure Vessel Steels. *Metals* **2023**, *13*, 1586. [CrossRef]
4. Zhu, X.; Liu, X.; Wang, R.; Li, Y.; Liu, W. Effects of Ar Ion Irradiation on Microstructure of Fe-Cu Alloys at 290 °C. *Acta Metall. Sin.* **2022**, *58*, 905–910. [CrossRef]

5. Kamboj, A.; Bachhav, M.N.; Dubey, M.; Almirall, N.; Yamamoto, T.; Marquis, E.A.; Odette, R. The effect of phosphorus on precipitation in irradiated reactor pressure vessel (RPV) steels. *J. Nucl. Mater.* **2023**, *585*, 154614. [CrossRef]
6. Kuleshova, E.A.; Gurovich, B.A.; Bukina, Z.V.; Frolov, A.S.; Maltsev, D.A.; Krikun, E.V.; Zhurko, D.A.; Zhuchkov, G.M. Mechanisms of radiation embrittlement of VVER-1000 RPV steel at irradiation temperatures of (50–400) °C. *J. Nucl. Mater.* **2017**, *490*, 247–259. [CrossRef]
7. Courilleau, C.; Radiguet, B.; Chaouadi, R.; Stergar, E.; Duplessi, A.; Pareige, P. Contributions of Ni-content and irradiation temperature to the kinetic of solute cluster formation and consequences on the hardening of VVER materials. *J. Nucl. Mater.* **2023**, *585*, 154616. [CrossRef]
8. Kamboj, A.; Almirall, N.; Yamamoto, T.; Tumey, S.; Marquis, E.A.; Odette, R. Dose and dose rate dependence of precipitation in a series of surveillance RPV steels under ion and neutron irradiation. *J. Nucl. Mater.* **2024**, *588*, 154772. [CrossRef]
9. Chaouadi, R.; Gérard, R. Neutron flux and annealing effects on irradiation hardening of RPV materials. *J. Nucl. Mater.* **2011**, *418*, 137–142. [CrossRef]
10. Kryukov, A.; Debarberis, L.; von Estorff, U.; Gillemot, F.; Oszvald, F. Irradiation embrittlement of reactor pressure vessel steel at very high neutron fluence. *J. Nucl. Mater.* **2012**, *422*, 173–177. [CrossRef]
11. Kolluri, M.; Martin, O.; Naziris, F.; D'Agata, E.; Gillemot, F.; Brumovsky, M.; Ulbricht, A.; Autio, J.m.; Shugailo, O.; Horvath, A. Structural MATerias research on parameters influencing the material properties of RPV steels for safe long-term operation of PWR NPPs. *Nucl. Eng. Des.* **2023**, *406*, 112236. [CrossRef]
12. Edmondson, P.D.; Parish, C.M.; Nanstad, R.K. Using complimentary microscopy methods to examine Ni-Mn-Si-precipitates in highly-irradiated reactor pressure vessel steels. *Acta Mater.* **2017**, *134*, 31–39. [CrossRef]
13. Miller, M.K.; Powers, K.A.; Nanstad, R.K.; Efsing, P. Atom probe tomography characterizations of high nickel, low copper surveillance RPV welds irradiated to high fluences. *J. Nucl. Mater.* **2013**, *437*, 107–115. [CrossRef]
14. Kuleshova, E.A.; Zhuchkov, G.M.; Fedotova, S.V.; Maltsev, D.A.; Frolov, A.S.; Fedotov, I.V. Precipitation kinetics of radiation-induced Ni-Mn-Si phases in VVER-1000 reactor pressure vessel steels under low and high flux irradiation. *J. Nucl. Mater.* **2021**, *553*, 153091. [CrossRef]
15. Bing, B.; Han, X.; Jia, L.; He, X.; Zhang, C.; Yang, W. Influence analysis of alloy elements on irradiation embrittlement of RPV steel based on deep neural network. *Int. J. Adv. Nucl. React. Des. Technol.* **2023**, *5*, 44–51. [CrossRef]
16. He, W.-k.; Gong, S.-y.; Yang, X.; Ma, Y.; Tong, Z.-f.; Chen, T. Study on irradiation embrittlement behavior of reactor pressure vessels by machine learning methods. *Ann. Nucl. Energy* **2023**, *192*, 109965. [CrossRef]
17. Wang, J.A.; Rao, N.S.V.; Konduri, S. The development of radiation embrittlement models for US power reactor pressure vessel steels. *J. Nucl. Mater.* **2007**, *362*, 116–127. [CrossRef]
18. Regulatory Guide. *Radiation Embrittlement of Reactor Vessel Materials (Revision 2)*; Nuclear Regulation Commission: Rockville, MD, USA, 1988.
19. Eason, E.D.; Odette, G.R.; Wright, J.E. *Improved Embrittlement CorrrE-Lations for Reactor Pressure Vessel Steels*; NUREG/CR-6551 Nuclear Regulatory Commission: Wastington, DC, USA, 1998.
20. *ASTM E900-15*; Standard Guide for Predicting Radiation-Induced Transition Temperature Shift in Reactor Vessel Materials. ASTM International: Conshohocken, PA, USA, 2017.
21. Tanon, A.; Grandemange, J.; Houssin, B.; Buchalet, C. *French Verification of PWR Vessel Integrity*; Electric Power Research Institute: Palo Alto, CA, USA, 1990.
22. *JEAC 4201*; Nuclear Reactor Pressure Vessel Structural Material Surveillance Test Method. JEAC: Tokyo, Japan, 1991.
23. Raccuglia, P.; Elbert, K.C.; Adler, P.D.F.; Falk, C.; Wenny, M.B.; Mollo, A.; Zeller, M.; Friedler, S.A.; Schrier, J.; Norquist, A.J. Machine-learning-assisted materials discovery using failed experiments. *Nature* **2016**, *533*, 73–76. [CrossRef]
24. Xie, J.; Su, Y.; Xue, D.; Jiang, X.; Fu, H.; Huang, H. Machine Learning for Materials Research and Development. *IMR* **2021**, *57*, 1343–1361. [CrossRef]
25. Liu, X.; Xu, P.; Zhao, J.; Lu, W.; Li, M.; Wang, G. Material machine learning for alloys: Applications, challenges and perspectives. *J. Alloys Compd.* **2022**, *921*, 165984. [CrossRef]
26. Castin, N.; Malerba, L.; Chaouadi, R. Prediction of radiation induced hardening of reactor pressure vessel steels using artificial neural networks. *J. Nucl. Mater.* **2011**, *408*, 30–39. [CrossRef]
27. Mathew, J.; Parfitt, D.; Wilford, K.; Riddle, N.; Alamaniotis, M.; Chroneos, A.; Fitzpatrick, M.E. Reactor pressure vessel embrittlement: Insights from neural network modelling. *J. Nucl. Mater.* **2018**, *502*, 311–322. [CrossRef]
28. Li, Y.; Jin, T.; Wang, Z.; Wang, D. Engineering critical assessment of RPV with nozzle corner cracks under pressurized thermal shocks. *Nucl. Eng. Technol.* **2020**, *52*, 2638–2651. [CrossRef]
29. Zheng, Y.; Wang, G.Z.; Tu, S.T.; Xuan, F.Z. Development of pressure-temperature limit curves considering unified constraint for reactor pressure vessel. *Int. J. Press. Vessel. Pip.* **2024**, *207*, 105117. [CrossRef]
30. Zhang, Z.; Ren, X.; Niu, Q.; Zhang, Y.; Zhao, B. Durability degradation simulation of RC structure based on gamma process considering two-dimensional chloride diffusion and life probabilistic prediction. *Structures* **2023**, *48*, 159–171. [CrossRef]
31. Chang, M.; Huang, X.; Coolen, F.P.A.; Coolen-Maturi, T. New reliability model for complex systems based on stochastic processes and survival signature. *Eur. J. Oper. Res.* **2023**, *309*, 1349–1364. [CrossRef]
32. Moran, P. Notes on continuous stochastic phenomena. *Biometrika* **1950**, *37*, 17–23. [CrossRef]
33. Abdel-Hameed, M. A Gamma Wear Process. *IEEE Trans. Reliab.* **1975**, *R-24*, 152–153. [CrossRef]

34. Strauss, A.; Wendner, R.; Vidovic, A.; Zambon, I.; Frangopol, D.M. Prediction of creep and shrinkage based on gamma process models. In Proceedings of the 12th International Conference on Applications of Statistics and Probability in Civil Engineering, ICASP12, Vancouver, BC, Canada, 12–15 July 2015.
35. Zhang, C.; Tee, K.F. Application of gamma process and maintenance cost for fatigue damage of wind turbine blade. *Energy Procedia* **2019**, *158*, 3729–3734. [CrossRef]
36. Kallen, M.J.; van Noortwijk, J.M. Optimal maintenance decisions under imperfect inspection. *Reliab. Eng. Syst. Saf.* **2005**, *90*, 177–185. [CrossRef]
37. Lawless, J.; Crowder, M. Covariates and Random Effects in a Gamma Process Model with Application to Degradation and Failure. *Lifetime Data Anal.* **2004**, *10*, 213–227. [CrossRef] [PubMed]
38. PLOTTER Database. Adjunct for e900-15 Technical Basis for the Equation Used to Predict Radiation-Induced Transition Temperature Shift in Reactor Vessel Materials. Available online: https://www.astm.org/adje090015-ea.html (accessed on 1 January 2015).
39. Qiangmao, W.; Guogan, S.; Rongshan, W.; Hui, D.; Ai, R.; Xiao, P.; Qi, Z.; Jing, L. Strategies for life management of French 900 MWe PWR RPV due to neutron irradiation embrittlement. *Nucl. Sci. Eng.* **2011**, *31*, 372–384.
40. Ballesteros, A.; Ahlstrand, R.; Bruynooghe, C.; Chernobaeva, A.; Kevorkyan, Y.; Erak, D.; Zurko, D. Irradiation temperature, flux and spectrum effects. *Prog. Nucl. Energy* **2011**, *53*, 756–759. [CrossRef]
41. Del Serrone, G.; Moretti, L. A stepwise regression to identify relevant variables affecting the environmental impacts of clinker production. *J. Clean. Prod.* **2023**, *398*, 136564. [CrossRef]
42. Ikotun, A.M.; Ezugwu, A.E.; Abualigah, L.; Abuhaija, B.; Heming, J. K-means clustering algorithms: A comprehensive review, variants analysis, and advances in the era of big data. *Inf. Sci.* **2023**, *622*, 178–210. [CrossRef]
43. Yu, Y.; Liu, M.; Chen, D.; Huo, Y.; Lu, W. Dynamic grouping control of electric vehicles based on improved k-means algorithm for wind power fluctuations suppression. *Glob. Energy Interconnect.* **2023**, *6*, 542–553. [CrossRef]
44. Pourshoaib, S.J.; Rajabzadeh Ghatrami, E.; Shamekhi, M.A. Comparing ultrasonic- and microwave-assisted methods for extraction of phenolic compounds from Kabkab date seed (*Phoenix dactylifera* L.) and stepwise regression analysis of extracts antioxidant activity. *Sustain. Chem. Pharm.* **2022**, *30*, 100871. [CrossRef]

Disclaimer/Publisher's Note: The statements, opinions and data contained in all publications are solely those of the individual author(s) and contributor(s) and not of MDPI and/or the editor(s). MDPI and/or the editor(s) disclaim responsibility for any injury to people or property resulting from any ideas, methods, instructions or products referred to in the content.